1-4-2018

An Intracellular Activation of Smoothened that is Independent of Hedgehog Stimulation in *Drosophila*

Kai Jiang
University of Kentucky, kai.jiang@uky.edu

Yajuan Liu
University of Kentucky, yajuan.liu@uky.edu

Jie Zhang
University of Kentucky, jie.zhang3@uky.edu

Jianhang Jia
University of Kentucky, Jianhang.jia@uky.edu

© 2018. Published by The Company of Biologists Ltd | Journal of Cell Science (2018) 131, jcs211367.doi:10.1242/jcs.211367

RESEARCH ARTICLE

An intracellular activation of Smoothened that is independent of Hedgehog stimulation in *Drosophila*

Kai Jiang, Yajuan Liu, Jie Zhang and Jianhang Jia*

ABSTRACT

Smoothened (Smo), a GPCR family protein, plays a critical role in the reception and transduction of Hedgehog (Hh) signal. Smo is phosphorylated and activated on the cell surface; however, it is unknown whether Smo can be intracellularly activated. Here, we demonstrate that inactivation of the ESCRT-III causes dramatic accumulation of Smo in the ESCRT-III/MVB compartment, and subsequent activation of Hh signaling. In contrast, inactivation of ESCRTs 0–II induces mild Smo accumulation in the ESCRT-III/MVB compartment. We provide evidence that Kurtz (Krz), the *Drosophila* β-arrestin2, acts in parallel with the ESCRTs 0-II pathway to sort Smo to the multivesicular bodies and lysosome-mediated degradation. Additionally, upon inactivation of ESCRT-III, all active and inactive forms of Smo are accumulated. Endogenous Smo accumulated upon ESCRT-III inactivation is highly activated, which is induced by phosphorylation but not sumoylation. Taken together, our findings demonstrate a model for intracellular activation of Smo, raising the possibility for tissue overgrowth caused by an excessive amount, rather than mutation of Smo.

KEY WORDS: ESCRT, Hh, Smo, Vps20, Vps32, Signal transduction

INTRODUCTION

Hedgehog (Hh) signaling controls organ development, tissue homeostasis and body patterning. Malfunction of Hh signaling causes birth defects as well as several types of cancer (Briscoe and Thérond, 2013; Jiang and Hui, 2008). In *Drosophila*, the Hh signal is transduced at the plasma membrane, where the receptor complex Patched–Interference Hh (Ptc–Ihog) and the signal transducer Smoothened (Smo) are located. Hh binding to Ptc–Ihog relieves Ptc-mediated inhibition of Smo, which results in Smo activation and then the activation of the Cubitus interruptus (Ci)/Gli family of zinc finger transcription factors, and ultimately induces the expression of Hh target genes, such as *decapentaplegic* (*dpp*), *ptc*, *collier* (*col*) and *engrailed* (*en*) (Hooper and Scott, 2005; Jia and Jiang, 2006). Smo is a member of the G protein-coupled receptor (GPCR) family and acts as a key regulator of the pathway for both insects and vertebrates. Abnormal activation of Smo results in basal cell carcinoma (BCC) and medulloblastoma; thus Smo has been an attractive therapeutic target exemplified by recent US Food and Drug Administration (FDA)-approved Smo inhibitors for treating cancer driven by Smo dysregulation (Pak and Segal, 2016).

Markey Cancer Center, Department of Molecular and Cellular Biochemistry, University of Kentucky College of Medicine, Lexington, KY 40536, USA.

*Author for correspondence (Jianhang.jia@uky.edu)

J.J., 0000-0002-9313-3843

Received 21 September 2017; Accepted 13 November 2017

Studies have shown that Hh induces cell surface accumulation and phosphorylation of Smo by protein kinase A (PKA), casein kinase 1 (CK1), casein kinase 2 (CK2), and G protein-coupled receptor kinase 2 (Gprk2) (Chen and Jiang, 2013; Jiang and Jia, 2015), as well as atypical PKC (aPKC) (Jiang et al., 2014). Differential phosphorylation and gradual conformational change in Smo mediates the transduction of Hh activity gradient (Fan et al., 2012; Zhao et al., 2007). The cell surface accumulation of Smo is also regulated by endocytosis; ubiquitylation promotes Smo endocytosis and de-ubiquitylation by Ubiquitin-specific protease 8 (USP8) inhibits Smo endocytosis, which ultimately promotes its cell surface accumulation (Li et al., 2012; Xia et al., 2012). Membrane accumulation and activation of Smo is further regulated by small ubiquitin-like modifier (SUMO) through sumoylation (Ma et al., 2016; Zhang et al., 2017). These findings indicate that cell surface accumulation promotes the activation of Smo; however, it is unknown whether and how Smo can be activated intracellularly.

Many GPCRs use the intracellular route to activate downstream genes. Studies on GPCRs have demonstrated that activation of receptors, and consequent activation of downstream components, often stimulate the receptor endocytosis (Irannejad and von Zastrow, 2014; Sorkin and von Zastrow, 2009). This process may function as a feedback regulation to prevent excessive ligand-induced activation of downstream effectors (Sorkin and von Zastrow, 2009). In addition, GPCR phosphorylation and their association with β-arrestins play a major role in this process (Irannejad and von Zastrow, 2014). Molecular sorting machineries determine their ultimate trafficking fate, as receptors either recycle back to the cell surface or are targeted for lysosomal degradation. Unlike other GPCRs, Smo is activated and accumulated on the cell surface upon Hh stimulation. It is unknown whether Smo undergoes intracellular signaling along the endocytic pathway.

The endosomal sorting complex required for transport (ESCRT) machinery includes four ESCRT complexes (ESCRT-0, -I, -II, -III) and Vacuolar protein sorting 4 (Vps4), and these machineries mediate the selection and transport of proteins destined for lysosomal degradation (Hurley and Hanson, 2010; Wollert and Hurley, 2010). ESCRT facilitates ubiquitylated protein trafficking from endosomes to lysosomes via multivesicular bodies (MVBs) (Henne et al., 2011; Raiborg and Stenmark, 2009; Williams and Urbé, 2007). Clathrin-dependent endocytosis mediates the activation of epidermal growth factor receptor (EGFR), which is further sorted to the MVB then is trafficked to the lysosome (Goh et al., 2010). The ESCRTs 0–III protein complexes drive MVB cargo selection; however, ESCRT-III does not directly interact with ubiquitin. Many membrane-bound proteins are actively sorted to different places in the cell from the early endosome (Hurley and Hanson, 2010). In *Drosophila* Smo trafficking, the homologs of the ESCRT members mediate sorting of ubiquitylated Smo to endosomes. Smo accumulation is observed upon the inactivation of the ESCRT proteins, such as the Hepatocyte growth factor-regulated

Journal of Cell Science (2018) 131, jcs211367. doi:10.1242/jcs.211367

tyrosine kinase substrate (Hrs), a protein that acts within ESCRT-0 (Fan et al., 2013; Li et al., 2012), Tumor susceptibility gene 101 (Tsg101) in ESCRT-I (Fan et al., 2013; Li et al., 2012), and Vps36 in ESCRT-II (Yang et al., 2013). However, inactivation of the proteins of the early endosome, late endosome, or the ESCRTs 0–II causes a mild accumulation of Smo, which is thought to contribute to the cell membrane accumulation and activation of Smo. It is unknown whether Smo can be activated in the intracellular compartments, similar to the activation of many other GPCRs.

In this study, we found that inactivation of the ESCRT-III core subunits, Vps32 (also known as Shrub in *Drosophila*, Snf7 in yeast, and CHMP4 in mammal) and Vps20 (CHMP6 in mammals), caused a dramatic increase in Smo. Surprisingly, inactivation of either Vps32 or Vps20 induced ectopic Hh target gene expression at higher levels compared to that induced by the inactivation of proteins in the ESCRTs 0–II. Furthermore, we found that Smo was activated in ESCRT-III-containing compartments, which did not rely on Hh stimulation and was not inhibited by Ptc, indicating that Smo activation can occur in an Hh- and Ptc-independent manner. Moreover, Smo ubiquitylation and sumoylation were not changed in ESCRT-III-containing compartments. To explore the mechanism for intracellular Smo accumulation, we identified a Krz-mediated pathway, operating in parallel to endocytosis, that directs Smo to the ESCRT-III complex and the MVB, which accounts for the high accumulation and activation of Smo. These findings indicate that Smo can be intracellularly activated, and that activated Smo at a certain threshold may result in high levels of Hh signaling activity.

RESULTS

Inactivation of ESCRT-III results in a high level of Smo and activates Hh target gene expression

Previous studies have shown that Smo undergoes lysosomal degradation that is triggered by ubiquitin-mediated endocytosis (Fan et al., 2013; Li et al., 2012; Xia et al., 2012). However, it has been puzzling that, in cultured S2 cells, the majority of Smo is present in large puncta that do not colocalize with ubiquitin (Fig. S1A). In *Drosophila* wing discs, the developing wing, posterior (P) compartment cells express and secrete Hh that activates adjacent anterior (A) compartment target gene expression, which is mediated by the Ci transcription factor. The low level of Smo in A-compartment cells away from the A/P boundary indicates a rapid protein degradation (Fig. 1A). In wing discs treated with bafilomycin A1 (BFA1) to selectively inhibit vacuolar ATPases that mediate the delivery of internalized proteins from MVB to lysosome, Smo was present in puncta in A- and P-compartment cells (Fig. S1C, compare to Fig. S1B), suggesting that Smo is indeed trafficked from the MVB to the lysosome for degradation. It is possible that the large puncta of Smo observed in S2 cells are located in larger intracellular compartments, such as the MVB.

To better understand the intracellular trafficking of Smo, we collected RNAi lines from different sources to target ESCRT protein expression. We found that knockdown of Vps32 by RNAi resulted in a high level of accumulation of Smo and Ci (Fig. S2A). The level of Ptc protein was also increased in A-compartment cells, indicating activation of the Hh pathway (Fig. S2B). To more precisely examine the accumulation of Smo in wing discs, we used either P35, a cell death inhibitor, or the inducible *Gal80*^{ts} system to prevent cell death induced by Vps32 RNAi. We found that Smo showed high levels of accumulation under both conditions (Fig. 1B, C, gray panel). We also found that the Smo accumulation caused by Vps32 RNAi in large part did not colocalize with Hrs (marks the ESCRT-0 complex) or Rab7 (marks the late endosome) (Fig. 1D; Fig. S2C), but mostly colocalized with lysosome-associated membrane protein 1 (LAMP1) (Fig. 1E), which labels the MVB and lysosome (Pulipparacharuvil et al., 2005; Williams and Urbé, 2007). The expression of LAMP1–GFP alone did not cause any phenotype *in vivo* (Pulipparacharuvil et al., 2005), and did not change Smo accumulation (Fig. S2D). GFP-tagged Vps32 (Vps32–GFP) has shown to be a dominant negative (Sweeney et al., 2006). We found that Vps32–GFP colocalized with Smo, and induced Smo and Ci accumulation in the wing disc, likely by blocking the function of endogenous Vps32 (Fig. S2E,F). These data suggest that the inactivation of Vps32 causes a dramatic accumulation of Smo, which is likely localized in the MVB.

To examine whether the inactivation of Vps32 regulates the activity of Smo, we first used a sensitized genetic background by expressing the partial dominant-negative Smo^{DN} that we previously described as Smo^{-PKA12}. In this protein, two PKA phosphorylation sites are mutated to avoid phosphorylation (Jia et al., 2004). Expressing Smo^{DN} through the wing-specific *C765*-Gal4, a weaker Gal4 line than *MS1096*-Gal4, resulted in a reproducible phenotype of partial fusion between vein 3 and vein 4, indicative of partial loss of Hh signaling activity (Fig. S2H, compare to WT wing in Fig. S2G). We found that Vps32 RNAi reversed the activity of Smo^{DN}, resulting in a rescue of the vein 3–vein 4 fusion phenotype (Fig. S2I). In comparison, Vps32 RNAi driven by C765-Gal4 produced a mild phenotype in the adult wing (Fig. S2J). These data indicate that inactivation of Vps32 regulates the activity of Smo. We further examined Smo accumulation in Vps32 mutant cells and found that Smo showed a dramatic accumulation in Vps32 mutant cells (Fig. 1F). Surprisingly, mutating Vps32 induced expression of En, a marker for the peak activation of Hh signaling (Fig. 1G). We next investigated cultured S2 cells and found that the levels of Smo were increased upon both Vps32 RNAi and Hh treatment, and that the accumulation of Smo reached a peak level when Vps32 RNAi and Hh treatment were combined (Fig. 1H). Consistent with this, Vps32 RNAi significantly increased the *ptc-luciferase* (*ptc-luc*) reporter activity, which was further increased upon Hh treatment (Fig. 1I). In these experiments, very high RNAi efficiency was achieved and monitored by quantitative real-time PCR (qRT-PCR) (Fig. 1J). In a cell-based assay to examine Smo cell surface accumulation, Hh treatment consistently increased the accumulation of Smo on the cell surface (Jia et al., 2004) (Fig. 1K); however, the inactivation of Vps32 significantly increased Smo accumulation inside the cell but not on the cell surface (Fig. 1K). These data suggest that Smo can be intracellularly activated during a malfunction of ESCRT-III.

To further examine the ESCRT-III-mediated regulation of Smo accumulation and activation, we used a mutant of Vps20, which is another critical protein in the ESCRT-III complex. We found a high accumulation of Smo in cells with mutated Vps20 (Fig. 2A). Consistent with the finding that mutating Vps32 induced Hh target gene expression (Fig. 1G), mutation of Vps20 induced ectopic expression of *dpp-lacZ* and *ptc-lacZ*, indicating that Smo activates Hh target gene expression in cell autonomous manner (Fig. 2B,C; Fig. S3 for higher magnification images). In cultured cells, we found that knockdown of Vps20 by RNAi significantly increased the *ptc-luc* activity (Fig. 1I); however, it did not increase the amount of cell surface-localized Smo (Fig. 1K). These data confirmed the activation of Smo upon ESCRT-III loss of function. These findings were very interesting because inactivation of the ESCRT-0, ESCRT-I and ESCRT-II increases the cell surface accumulation of Smo but does not significantly increase Hh target gene expression

Journal of Cell Science (2018) 131, jcs211367. doi:10.1242/jcs.211367

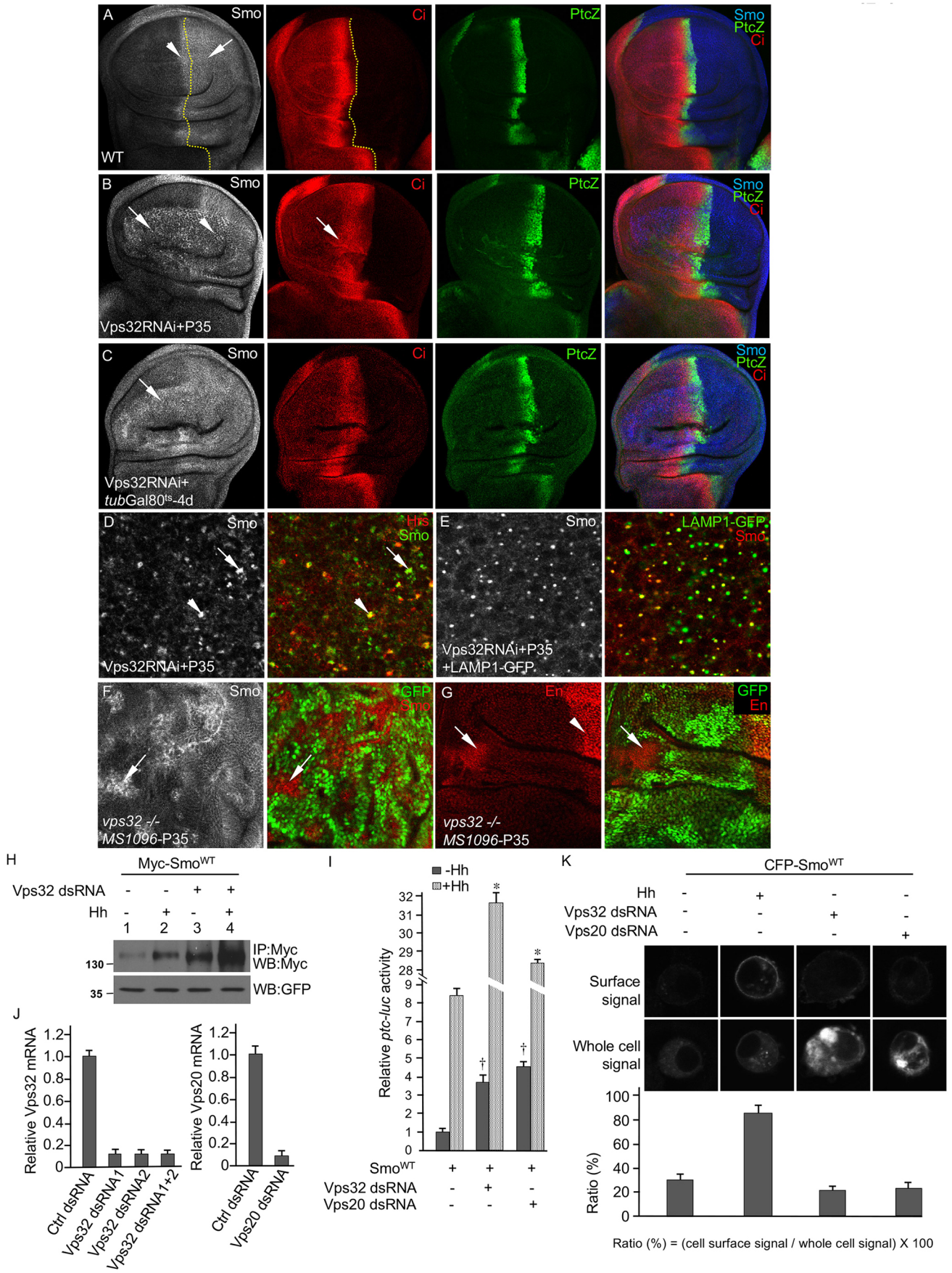

Fig. 1. See next page for legend.

Fig. 1. Inactivation of Vps32 induces the accumulation of Smo and the activation of Hh target gene expression. (A) A wild-type wing disc was immunostained for Smo, Ci and ptc-lacZ (PtcZ). Smo is stabilized in P-compartment cells (arrow) as well as A-compartment cells near the A/P boundary (arrowhead) where Hh stimulation occurs. The dashed yellow line indicates the A/P boundary as defined by Ci staining. (B) A wing disc from flies expressing *UAS-Vps32RNAi* and *UAS-P35* from the wing-specific *MS1096*-Gal4 at 19°C was immunostained for Smo, Ci, and ptc-lacZ. Arrows indicate the accumulation of Smo (gray) and Ci (red) in A-compartment cells, and the arrowhead indicates Smo accumulation in P-compartment cells. (C) A wing disc expressing *UAS-Vps32RNAi* driven by *MS1096*-Gal4 together with *tub-Gal80^{ts}* for 4 days at 29°C (non-permissive temperature) to inhibit Gal80 expression was stained for Smo, Ci and ptc-lacZ. The arrow indicates the accumulation of Smo in A-compartment cells. The mild accumulation of Ci shown in B and C was either due to the low temperature or the short time of induction. (D) A high-magnification image from a wing disc expressing *UAS-Vps32RNAi* and *UAS-P35* driven by *MS1096*-Gal4 and immunostained for Smo and Hrs. The arrowhead indicates Smo colocalization with Hrs and the arrow indicates the non-Hrs-colocalized Smo. (E) A high-magnification image from a wing disc expressing *UAS-Vps32RNAi* and *UAS-P35* together with *UAS-LAMP1-GFP* driven by *MS1096*-Gal4 and immunostained for Smo and GFP. (F,G) Wing discs carrying *vps32* mutant clones generated by flippase-mediated mitotic recombination were immunostained for Smo, En and GFP. Clones are marked by the lack of GFP expression. The arrows indicate the accumulation of Smo and the expression of En in *vps32*$^{-/-}$ cells; the arrowhead shows En expression induced by Hh in P-compartment cells. P35 was expressed through the *MS1096*-Gal4 to inhibit cell death. (H) S2 cells were transfected with Myc–Smo^{WT} and treated with Vps32 dsRNA or HhN-conditioned medium. Cell extracts were immunoprecipitated (IP) and analyzed by western blotting (WB) using the anti-Myc antibody to examine the levels of Smo. Western blots stained with the anti-GFP antibody served as a transfection and loading control. (I) A *ptc-luc* reporter assay to examine Hh signaling activity. S2 cells were transfected with Myc–Smo^{WT} and *tub*-Ci, and treated with HhN-conditioned medium or control medium, together with the treatment of Vps32 dsRNA or Vps20 dsRNA. The *y*-axis represents normalized *ptc-luc* activity. $^{\dagger}P<0.005$ versus Smo^{WT} expression alone in the first column (Student's *t*-test). $^{*}P<0.005$ versus Smo^{WT} treated with Hh in the second column (Student's *t*-test). (J) RNAi efficiency for Vps32 and Vps20. For Vps32 RNAi targeting different regions of Vps32, dsRNA1 and dsRNA2 alone or together gave rise to similar knockdown efficiency, thus dsRNA1 was used for most of the experiments. (K) S2 cells were transfected with the CFP-Smo construct, treated with Hh-conditioned medium or control medium, or treated with the indicated dsRNA of Vps32 and Vps20, followed by immunostaining with the anti-SmoN antibody before membrane permeabilization to label cell surface-localized Smo (top panel of cells). The CFP signal indicates the total Smo expressed (whole cell signal). A quantification of the cell surface to total Smo levels as a percentage is shown ($n\geq15$; mean±s.d.).

(Fan et al., 2013; Li et al., 2012; Yang et al., 2013), and we therefore did not expect Smo to be activated in the intracellular compartment.

Smo is phosphorylated and activated in ESCRT-III-containing compartments

To determine the active/inactive status of Smo in the intracellular compartment, we first examined the ability of Ptc to inhibit Smo activation. We found that overexpression of Ptc inhibited Smo accumulation and decreased the level of Ci in wild-type cells of the wing disc but not in Vps20-depleted cells (Fig. 2D). We also examined the levels of endogenous Ptc protein and found that Ptc accumulated upon Vps20 mutation (Fig. 2E); however, the accumulated Ptc, similar to exogenously expressed Ptc protein, did not inhibit Smo (Fig. 2A). These data suggest that the accumulation of Smo in the ESCRT-III-containing/MVB compartment is not inhibited by Ptc. To further examine the localization of Smo, we immunostained the wing disc for Vps4 that labels protein localization close to the ESCRT-III/MVB (Rodahl et al., 2009). We found that Smo colocalized with Vps4 in cells mutating Vps20 (Fig. 2F). Taken together with the finding that RNAi interference of Vps32 led to the accumulation of Smo (in puncta marked by LAMP1), our data suggest that the inactivation of ESCRT-III causes Smo accumulation in the MVBs.

To delineate whether the activation of Smo upon inactivation of ESCRT-III required Hh stimulation, we simultaneously inactivated both Hh and Vps32 and examined Smo accumulation in the wing disc. We found that Vps32 RNAi consistently increased Smo accumulation and induced ectopic *ptc-lacZ* expression regardless of the presence or absence of Hh RNAi (Fig. 3B, compared to Fig. 3A and Fig. S2A), suggesting that the intracellular activation of Smo does not rely on Hh stimulation. Hh RNAi alone blocked Smo accumulation and inhibited *ptc-lacZ* expression (Fig. 3C). To determine whether Smo existed in an active form, we performed immunostaining with an antibody against phosphorylated Smo (denoted SmoP) to examine Smo phosphorylation in the wing disc. Exogenous Myc–Smo^{WT} was expressed in the wing disc because the anti-SmoP antibody is unable to detect the phosphorylation of endogenous Smo. Consistent with previous findings (Fan et al., 2012), phosphorylated Smo was detected in P-compartment cells where there was Hh stimulation (Fig. 3D). We found that inactivation of Vps32 by RNAi increased the levels of Smo phosphorylation in the P-compartment cells as well as in the A-compartment cells away from the A/P boundary, suggesting an Hh-independent phosphorylation of Smo (Fig. 3E). We again used a cell-based assay to examine the levels of Smo phosphorylation and found that RNAi of Vps32 increased Smo phosphorylation, which was similar to what was seen upon Hh treatment (Fig. 3F). These data suggest that the Smo that accumulates upon Vps32 RNAi is in its active forms.

Recent studies have demonstrated that Smo is activated by sumoylation that is induced by Hh (Ma et al., 2016; Zhang et al., 2017). We therefore wondered whether the intracellularly accumulated Smo was sumoylated. Using the cell-based assay, we found that, in contrast to Hh treatment, inactivation of Vps32 by RNAi did not change the status of Smo sumoylation (Fig. 3G), suggesting that the inactivation of Vps32 increases the levels of Smo and induces Smo phosphorylation that ultimately promotes Hh signaling. We also examined the ubiquitylation status of Smo and found that knockdown of Vps32 by RNAi did not change the levels of ubiquitylation for either wild-type Smo (Smo^{WT}) or the phosphorylation-mimetic active form of Smo (Smo^{SD123}) (Fig. 3H). These findings suggest that intracellular Smo activation does not require sumoylation and is not mediated by deubiquitylation, pointing to a different mechanism from that utilized for cell membrane Smo activation.

Inactivation of ESCRT-III results in an accumulation of different forms of Smo

The unchanged levels of Smo sumoylation and ubiquitylation upon Vps32 inactivation led us to examine the stability of the different forms of Smo to determine which form of Smo accumulates in the ESCRT-III-containing compartment. We carried out a protein stability analysis by transfecting S2 cells with Myc–Smo^{WT}, Myc–Smo^{PKA123} (the phosphorylation-deficient, inactive form of Smo) and Myc–Smo^{SD123}, and then monitoring Smo levels upon the inactivation of Vps32. We then performed western blot analysis to examine the stability of the different forms of Smo and found that knockdown of Vps32 by RNAi increased the levels of all forms of Smo (Fig. 4A). We further found that the ubiquitylation-deficient forms of Smo [Smo^{K6R}, Smo^{K42R} and Smo^{KallR} (described by Yang et al., 2013)], were all increased upon Vps32 RNAi (Fig. 4B). These data suggest that ESCRT-III regulates different forms of Smo. We

Journal of Cell Science (2018) 131, jcs211367. doi:10.1242/jcs.211367

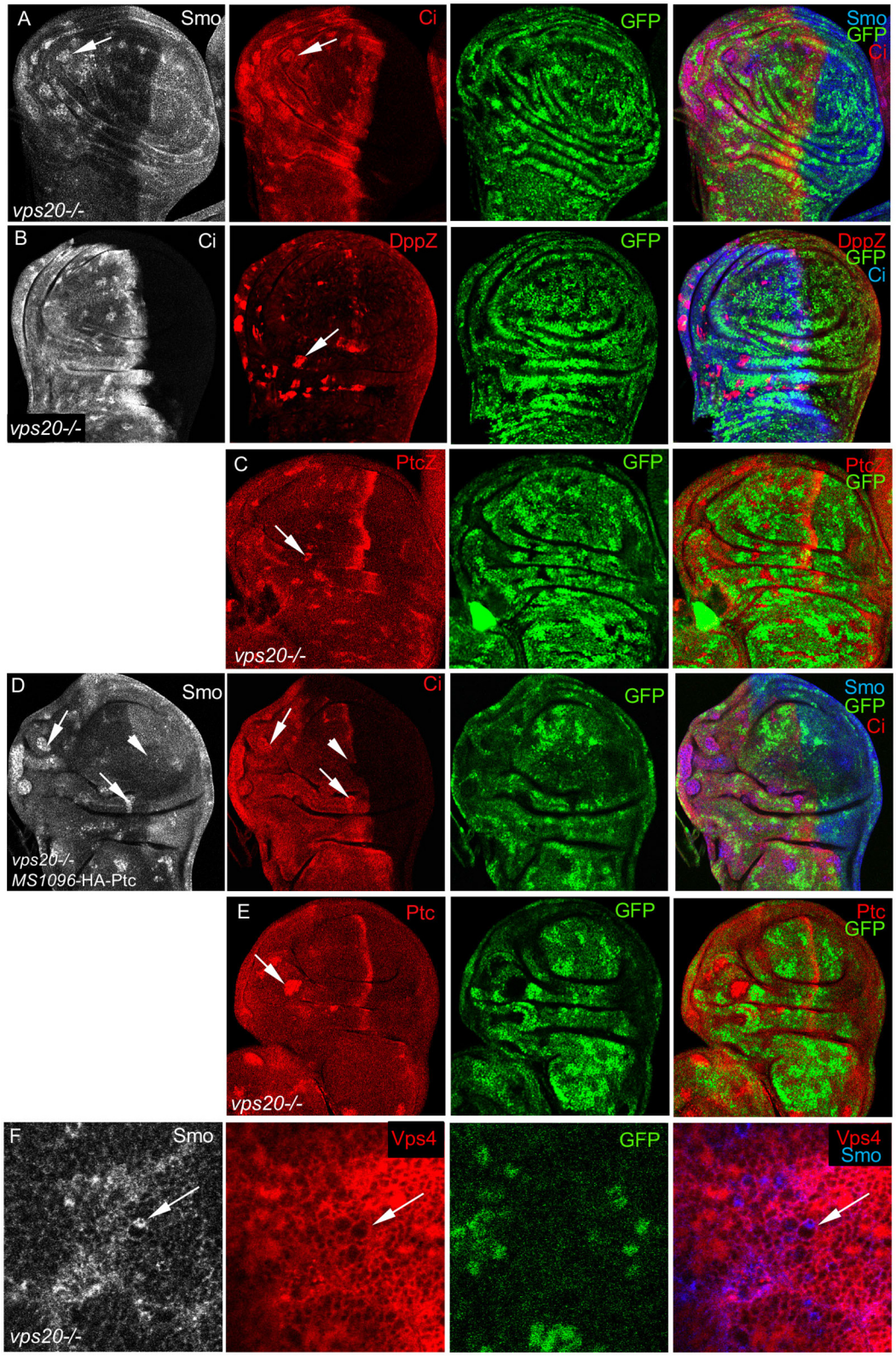

Fig. 2. Vps20 loss-of-function induces high levels of Smo accumulation and Hh signaling activation. (A) A wing disc carrying *vps20* mutant clones was immunostained for Smo, Ci and GFP. Clones are marked by the lack of GFP expression. Arrows indicate high accumulation of Smo and Ci. (B,C) Wing discs carrying *vps20* mutant clones were immunostained for GFP, dpp-lacZ (DppZ) or ptc-lacZ (PtcZ). The arrows identify the ectopic expression of *dpp-lacZ* and *ptc-lacZ*. (D) A wing disc carrying *vps20* mutant clones and expressing *UAS-HA-Ptc* driven by *MS1096*-Gal4 was immunostained for Smo, Ci and GFP. The arrows show a high accumulation of Smo and Ci not inhibited by Ptc expression in *vps20* mutant cells. The arrowheads identify the inhibition of Smo and Ci accumulation in *vps20* wild-type cells. (E) A wing disc carrying *vps20* mutant clones was immunostained for Ptc and GFP. The arrow indicates a high accumulation of Ptc protein. (F) High-magnification of a wing disc carrying *vps20* mutant clones and immunostained for Smo, Vps4, and GFP. Arrows indicate the colocalization of Smo with Vps4.

Journal of Cell Science (2018) 131, jcs211367. doi:10.1242/jcs.211367

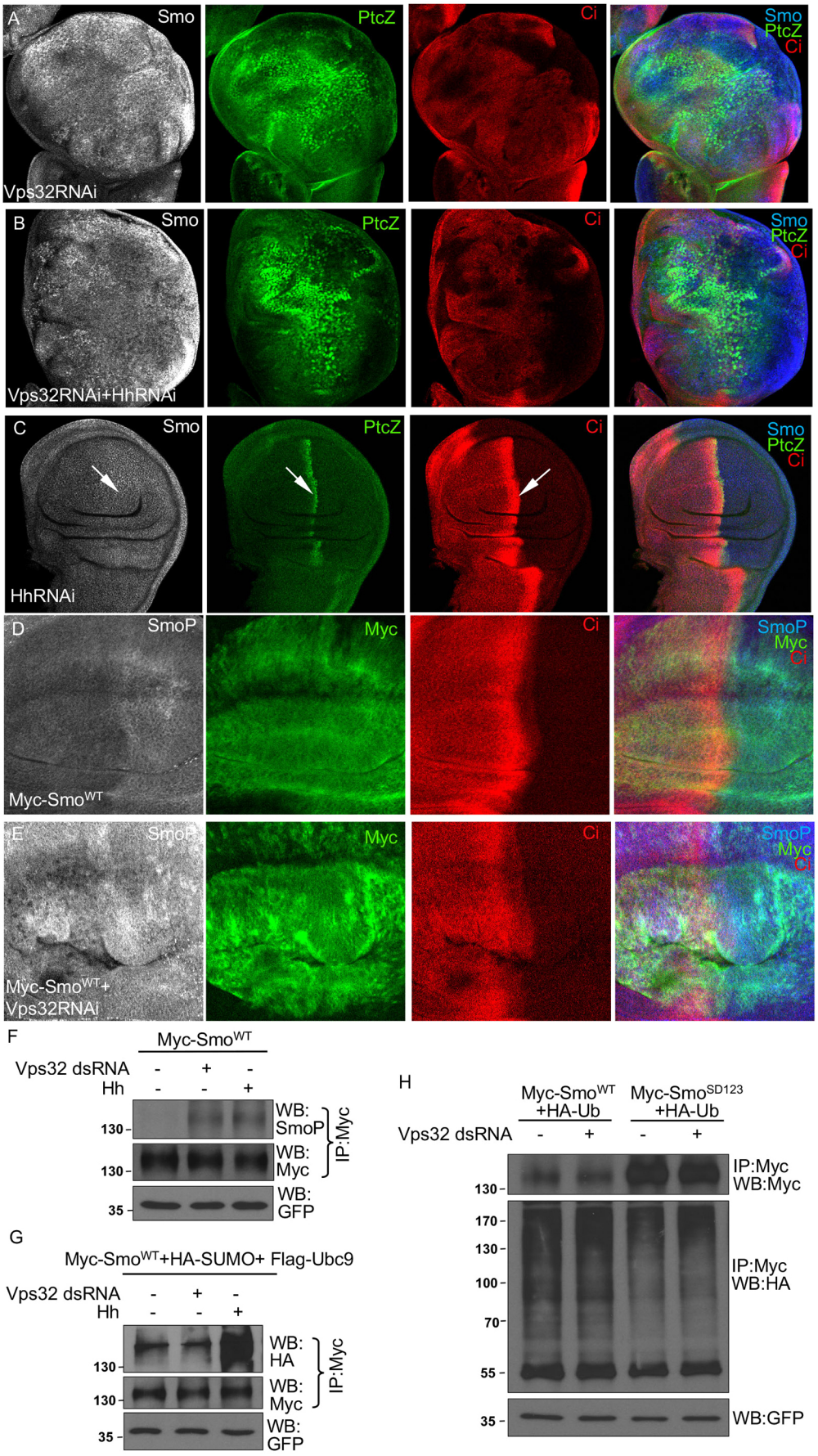

Fig. 3. Smo is phosphorylated and activated by Vps32RNAi in wing disc. (A–C) Wing discs from flies expressing *UAS-Vps32RNAi* and *UAS-HhRNAi* alone or together driven by *MS1096*-Gal4 were stained for Smo, ptc-lacZ (PtcZ) and Ci. A control experiment is shown in C, with arrows indicating the blocked accumulation of Smo (arrow in gray image), inhibited expression of ptc-lacZ (arrow in green image) and inhibited activation of Ci (arrow in red image). Of note, co-expressing Vps32RNAi with HhRNAi caused a very similar phenotype to that seen upon expressing Vps32RNAi alone. (D,E) Higher magnification images of wing discs from flies expressing Myc–Smo^{WT} alone or together with Vps32 RNAi. Discs were immunostained with the anti-Myc, anti-Ci and anti-SmoP antibodies. Of note, the anti-SmoP antibody can detect phosphorylation of the overexpressed Smo. (F) S2 cells were transfected with Myc–Smo^{WT} followed by the treatment with Vps32 dsRNA or HhN-conditioned medium. Cell extracts were immunoprecipitated (IP) with the anti-Myc antibody and analyzed by western blotting (WB) using either the anti-SmoP antibody to detect Smo phosphorylation or the anti-Myc antibody to monitor the expression of Myc–Smo^{WT}. Western blots for GFP served as a transfection and loading control. Smo was normalized by previously described methods (see Materials and Methods). (G) A cell-based assay to detect the levels of Smo sumoylation. S2 cells were co-transfected with Myc–Smo^{WT}, HA–SUMO and Flag–Ubc9, followed by the treatment with Vps32 dsRNA, HhN-conditioned medium or control medium. Cell extracts were immunoprecipitated with the anti-Myc antibody and analyzed by western blotting using the anti-HA antibody to examine the Smo-bound SUMO, or with the anti-Myc antibody to monitor the levels of Smo. Western blots for GFP served as a transfection and loading control. Smo was normalized by the previously described methods (see Materials and Methods). (H) To examine Smo ubiquitylation, S2 cells were transfected with the indicated constructs followed by treatment with Vps32 dsRNA. Cell lysates were immunoprecipitated with the anti-Myc antibody and analyzed by western blotting using the anti-HA antibody to examine the Smo-bound ubiquitin, or with the anti-Myc antibody to monitor the levels of Smo. Western blots for GFP served as a transfection and loading control. Myc–Smo^{WT} and Myc–Smo^{SD123} were normalized separately.

Journal of Cell Science (2018) 131, jcs211367. doi:10.1242/jcs.211367

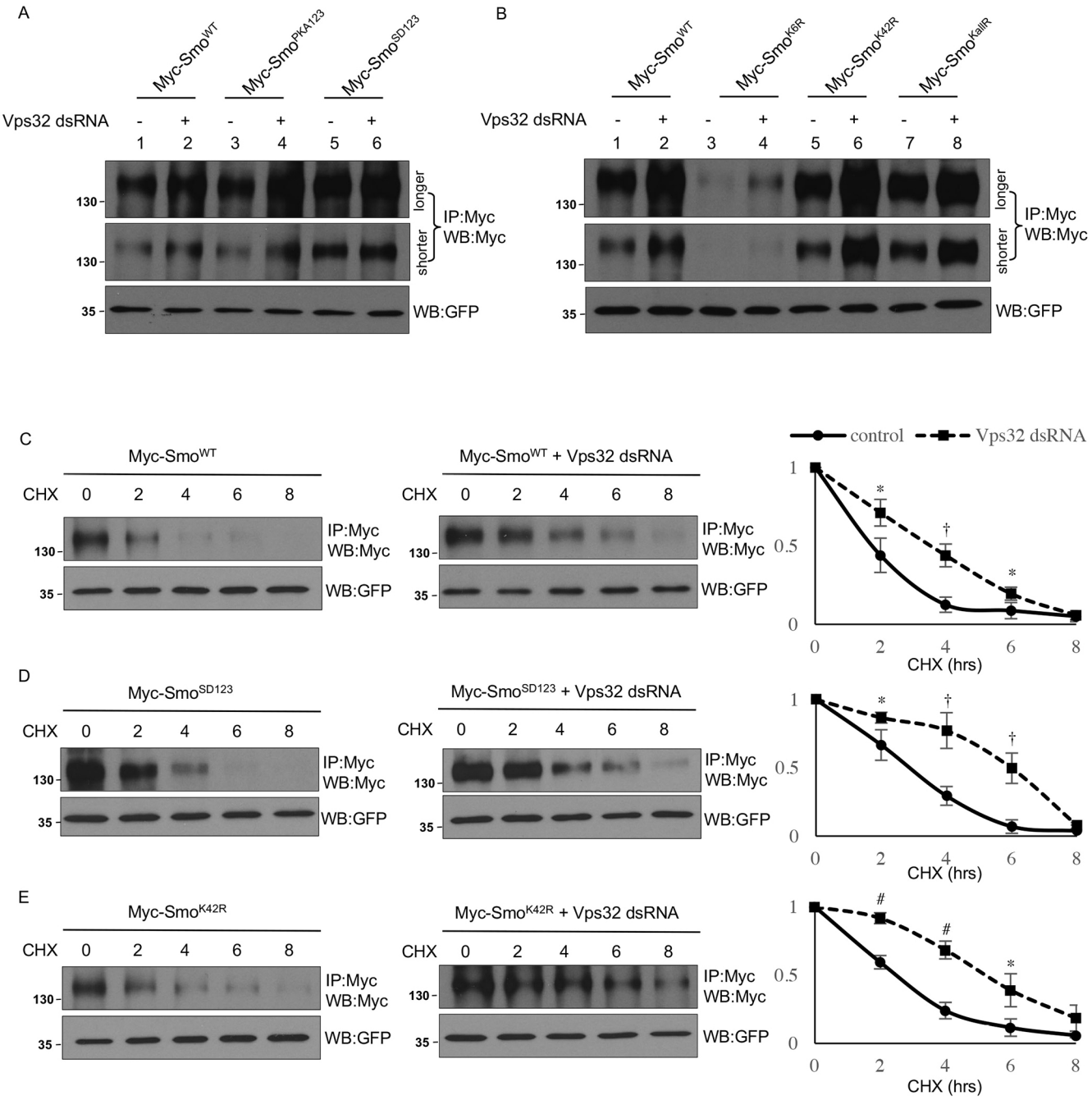

Fig. 4. The stability of Smo variants regulated by the inactivation of Vps32. (A,B) S2 cells were transfected with the indicated Smo constructs followed by the treatment with Vps32 dsRNA. Cell extracts were immunoprecipitated with the anti-Myc antibody and analyzed by western blotting with the anti-Myc antibody to examine the stability of Smo. For a better comparison, images from shorter and longer exposure times are shown. Western blots for GFP served as a transfection and loading control. (C–E) Smo protein stability assays. S2 cells were transfected with Myc–Smo^{WT}, Myc–Smo^{SD123} or Myc–Smo^{K42R}, treated with or without Vps32 dsRNA, and incubated with CHX for the indicated time periods. Cell extracts were immunoprecipitated with the anti-Myc antibody and analyzed by western blotting with the anti-Myc antibody to examine the levels of Smo protein. The quantification of Smo levels at different time points are shown in the right panel. Signal density at t=0 was defined as 100%. Data were from three independent experiments for each set. *P<0.05, †P<0.01, #P<0.001 versus Smo expression without Vps32 dsRNA (Student's t-test).

therefore performed a more precise analysis to examine the stability of the Smo protein at different time points after the treatment by using the protein synthesis inhibitor cycloheximide (CHX). We found that the half-lives of Smo^{WT} and Smo^{SD123} were increased upon Vps32 RNAi (Fig. 4C,D, middle panel), compared to the half-lives of these forms of Smo in cells without Vps32 knockdown (Fig. 4C,D, left panel), which was further demonstrated by quantification analyses (Fig. 4C,D, right panel). These data suggest that the active form of Smo is sorted through ESCRT-III for lysosome-mediated degradation.

It has been shown that ubiquitylation at lysine residues of Smo C-tail promotes, whereas mutating these residues blocks, Smo endocytosis (Li et al., 2012; Xia et al., 2012; Yang et al., 2013). Interestingly, we found that Smo^{K42R}, with all 42 lysine residues in the Smo C-tail mutated to arginine to block Smo ubiquitylation, accumulated in *vps20* mutant cells (Fig. 5B), which was similar to

Journal of Cell Science (2018) 131, jcs211367. doi:10.1242/jcs.211367

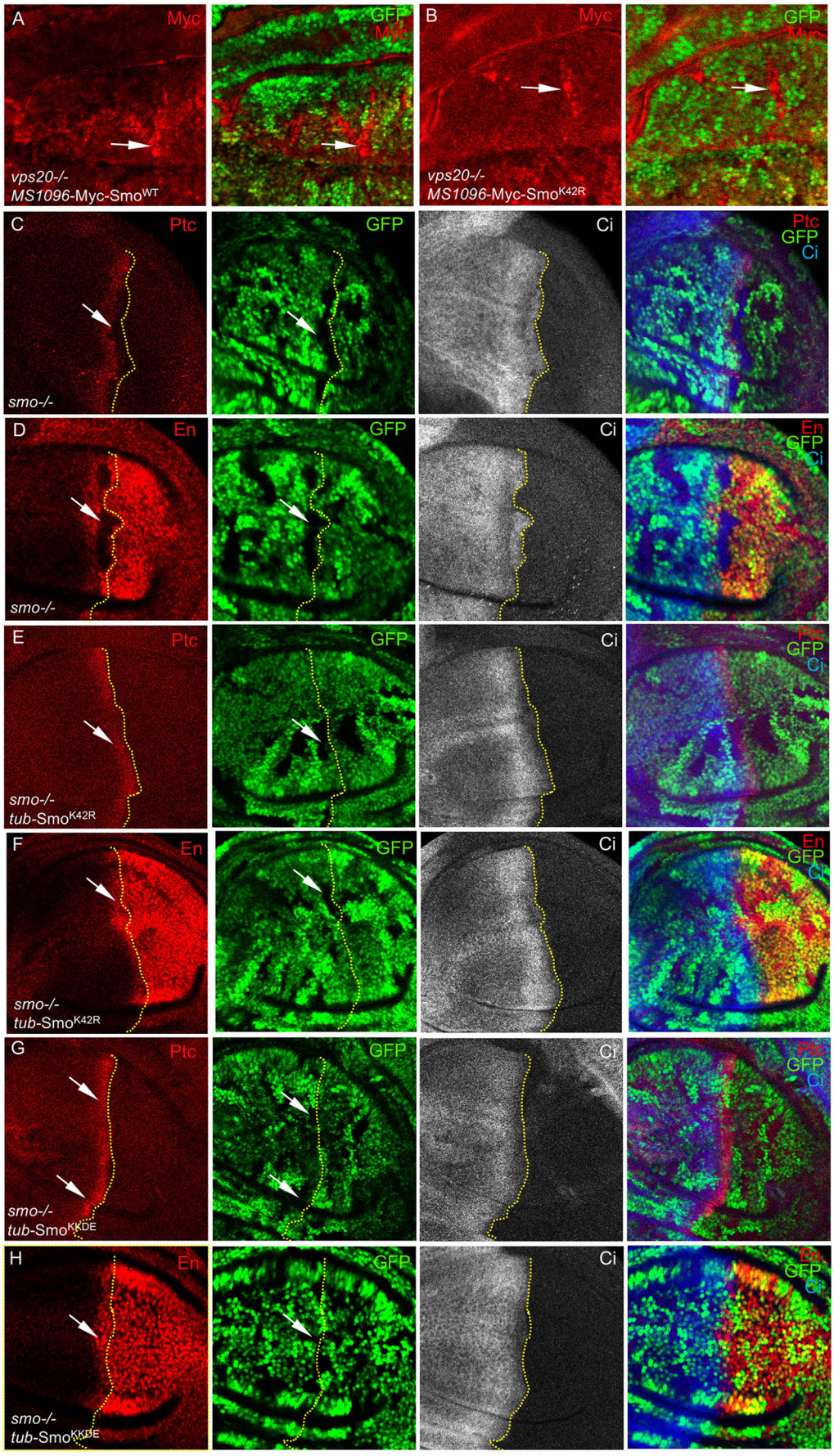

Fig. 5. The signaling activity of different forms of Smo *in vivo*. (A,B) Wing discs carrying *vps20* mutant clones and expressing Myc–Smo^{WT} or Myc–Smo^{K42R} driven by *MS1096*-Gal4 were immunostained for GFP to label the clones, and for Myc to examine the levels of Smo inside and outside *vps20* clones. The arrows indicate the elevated levels of both Smo^{WT} and Smo^{K42R} in cells with mutated *vps20*. (C,D) Wing discs carrying *smo* mutant clones immunostained for Ptc, En, Ci and GFP. Arrows in the red panel indicate the lack of Ptc or En expression upon *smo* mutation. Arrows in the green panel indicate the clones recognized by the lack of GFP expression. (E–H) Wing discs containing *smo* mutant clones and expressing different forms of Smo at the same attP locus (VK5 75B1) driven by the *tubulin-*α promoter were immunostained for Ptc, En, Ci and GFP. Arrows in the red panel indicate the rescue of Ptc or En expression by the exogenously expressed Smo. Arrows in the green panel show *smo* mutant clones marked by the lack of GFP expression. Yellow dashed lines indicate the A/P boundary defined by Ci staining.

the observed accumulation of Smo^{WT} in these cells (Fig. 5A). Both Smo^{WT} and Smo^{K42R} were stabilized by the treatment of BFA1 in cultured S2 cells (data not shown). These data suggest that Smo^{K42R} is sorted into the ESCRT-III-containing/MVB compartment through a different route rather than through the endocytosis pathway. In support of this hypothesis, the half-life of Smo^{K42R} was increased by knockdown of Vps32 in the cell-based assay that focused on Smo stability (Fig. 4E). To examine the *in vivo* activity of Smo^{K42R}, we used the *tubulin-α* promoter, which gives an expression level that is similar to the endogenous Smo expression level (Jia et al., 2010), and found that Smo^{K42R} rescued *ptc* and *en* expression in *smo* mutant cells (Fig. 5E,F, compare to 5C and 5D, respectively). The activity of Smo^{K42R} may have two components: one from Smo accumulation on the membrane due to the blockade of endocytosis, and the other from the accumulation in the ESCRT-III-containing/MVB compartment.

Many membrane-bound proteins contain a KKDE motif that interacts with COP-I coats, which mediate target protein delivery to the endoplasmic reticulum. Fusion of the KKDE motif at the C-terminus of Smo removed Smo from the cell surface and significantly reduces the activity level of the different forms of Smo (Zhu et al., 2003). To further assess the role of the intracellularly localized Smo in transducing an Hh signal, we generated Smo^{KKDE}, with a fused KKDE motif at the C-terminus, under the control of the *tubulin-α* promoter. We found that Smo^{KKDE} was able to rescue both Ptc and En expression in *smo* mutant cells (Fig. 5G,H). The FDNPVY internalization signal from the LDL receptor is a motif known to promote protein endocytosis (Wang and Struhl, 2004). We fused a 23-amino-acid peptide that contains the FDNPVY signal to the C-terminus of Smo (Smo^{FD}). We found that, driven by the *tubulin-α* promoter, Smo^{FD} fully rescued both Ptc and En expression (Fig. S4A,B). Compared to Smo^{WT}, both Smo^{KKDE} and Smo^{FD} showed a significant reduction in cell surface accumulation even when there was Hh stimulation (Fig. S4C). These data suggest that forcing Smo to localize to the intracellular compartment does not alter its ability to induce Hh target gene expression, demonstrating the signaling activity of intracellularly localized Smo.

Krz acts in parallel to the endocytosis pathway to sort Smo to ESCRT-III

Hrs and Signal transducing adaptor molecule (Stam) constitute the ESCRT-0 complex responsible for the initial selection of ubiquitylated proteins that are ultimately degraded in lysosomes (Henne et al., 2011). We found that RNAi-mediated knockdown of Hrs caused a mild increase in Smo accumulation (Fig. 6C, compared to 6A), which is consistent with previous findings (Fan et al., 2013; Li et al., 2012). We also found a mild accumulation of Smo in *hrs* mutant cells (Fig. S6A), and that the double mutation of *hrs* and *stam* did not increase the accumulation of Smo (Fig. S6B). Doubly mutating *hrs* and *stam* was thought to completely block Smo endocytosis mediated by ESCRT-0. Our findings raise the possibility that Smo, especially the non-ubiquitylated forms of Smo, undergoes trafficking/degradation through other mechanisms.

Previous studies showed that Kurtz (Krz), the *Drosophila* non-visual arrestin, downregulated Smo accumulation by promoting Smo degradation in a ubiquitin- and Gprk2-independent manner (Li et al., 2012; Molnar et al., 2011). Overexpression of Krz prevented Smo accumulation in wing discs but *krz* mutation did not (Fig. 6E) (Li et al., 2012; Zhang et al., 2017). Similarly, we found that knockdown of Krz by RNAi did not result in any change in Smo accumulation (Fig. 6B, compared to 6A). However, Smo accumulation was markedly increased when Krz RNAi and Hrs RNAi were combined (Fig. 6D, compared to 6B and 6C). In addition, knockdown of Hrs by RNAi in *krz* mutant cells resulted in the accumulation of Smo to a higher level thatn in *krz* wild-type cells (Fig. 6F). It has been shown that Vps32 acts as a key modulator in ligand-independent Notch signaling mediated by Krz and ESCRT-III (Hori et al., 2011). Our findings led to the hypothesis that Krz and Hrs act in parallel pathways to regulate Smo trafficking. To further test this hypothesis, we examined the ability of Krz to inhibit Smo accumulation under a variety of conditions. We found that, consistent with previous findings, Krz overexpression completely blocked Smo accumulation (Fig. 6G). Hrs RNAi caused Smo accumulation in both Krz-expressing cells (Fig. 6H) and wild-type cells (Fig. 6H,I). Furthermore, overexpression of Krz inhibited Smo accumulation in wild-type cells but not in *hrs* mutant cells (Fig. 6K). These results indicate that Hrs and Krz act in parallel to regulate Smo.

To determine how ESCRT-I regulates Smo, we examined the effect of Vps28 loss of function in the ESCRT-I complex. We found that mutating *vps28* induced a moderate accumulation of Smo, similar to that caused by *hrs* mutation (Fig. S6C and A, respectively). The accumulation of Smo in *vps28* mutant cells was not adequate to induce Ci accumulation in the wing disc (Fig. S6C). These data indicate that the same forms of Smo are trafficked from ESCRT-0- to ESCRT-I-containing compartments. Our finding that both RNAi and mutation of Vps32 caused a striking accumulation of Smo in the ESCRT-III-containing compartment (Figs 1 and 2) suggests that Smo may sort to the ESCRT-III through an ESCRT-0-independent pathway. In support of this hypothesis, we found that Krz overexpression did not inhibit the Smo accumulation that was induced by Vps32 RNAi (Fig. 6J). The Vps4 complex acts downstream of ESCRT-III to mediate protein degradation through lysosomes. Similar to what was seen with Vps32 RNAi (Fig. 3A; Fig. S2A), Smo accumulation was observed when a dominant-negative $Vps4^{DN}$ was expressed in wing disc (Fig. S6D). Taken together, our data suggest that the parallel pathways mediated by Krz and Hrs may merge at ESCRT-III to direct additional trafficking and lysosomal degradation.

Autophagy is an evolutionarily conserved, highly regulated cellular process. Autophagosomes can potentially fuse with lysosomes, or with early and late endosomes; however, Vps34 and Beclin 1 play selective roles in the autophagy pathway (Funderburk et al., 2010; Raiborg and Stenmark, 2009). To examine whether Smo is regulated by the autophagy, we examined the accumulation of Smo in both wing disc and cultured S2 cells when autophagy gene expression was knocked down by RNAi. We found that knockdown of either Vps34 or Beclin 1 by RNAi did not cause any changes in Smo accumulation or *ptc-lacZ* expression in wing disc, although both Vps34 and Beclin 1 RNAi induced phenotypes in the adult wing (Fig. S5A,B, data not shown). Consistent with this, inactivation of other autophagy genes, such as Vps15, Atg8a, Atg8b and Atg7, did not cause any changes in Smo accumulation and Hh target gene expression (data not shown). The phenotypes are unlikely to be due to off-target effects because different lines targeting non-overlapping regions produced similar phenotypes. We also used the cell-based assay to examine Smo stability in S2 cells and found that RNAi for Vps15, Beclin1 and Vps34 did not cause any changes in the levels of Smo (Fig. S5C). Taken together, we conclude that the autophagy pathway is not involved in Smo stability control.

There is a possibility for Krz to mediate Smo degradation through the proteasome (Li et al., 2012). The dilemma was to be able to distinguish Krz-mediated Smo sorting to the MVB from that to the

Journal of Cell Science (2018) 131, jcs211367. doi:10.1242/jcs.211367

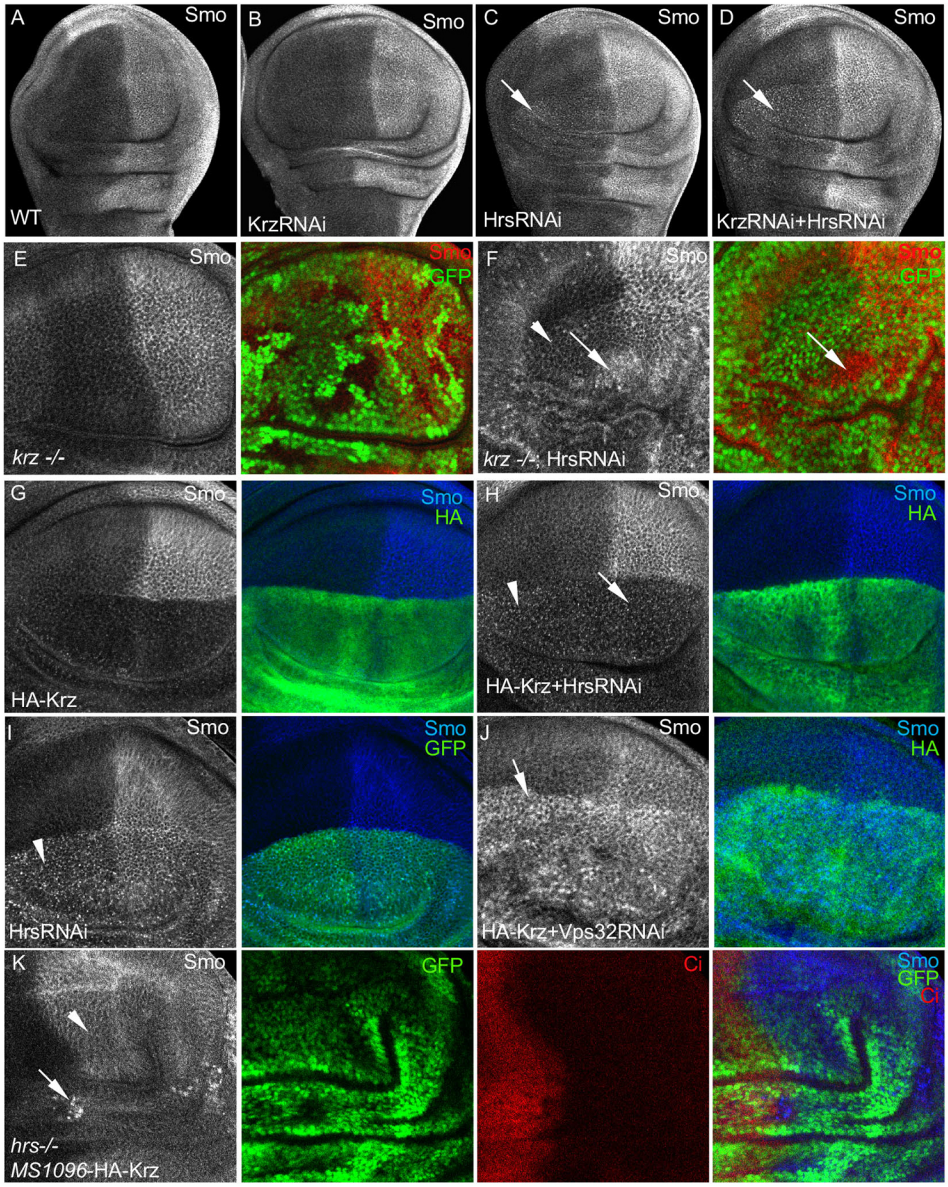

Fig. 6. Krz acts in parallel with the ESCRT-0 to promote trafficking. (A) A wing disc from wild-type flies immunostained for Smo. Smo accumulates in P-compartment cells where there is Hh stimulation. (B–D) Wing discs from flies expressing *UAS-KrzRNAi* and *UAS-HrsRNAi* driven by *MS1096*-Gal4 were stained for Smo. Arrows indicate the accumulation of Smo in A-compartment cells away from the A/P boundary. (E,F) Wing discs carrying *krz* mutant clones with or without the expression of HrsRNAi drievn by *MS1096*-Gal4 were stained for Smo and GFP. Arrows indicate the high accumulation of Smo in *krz* mutant cells expressing Hrs RNAi. The arrowhead indicates mild accumulation of Smo upon Hrs RNAi expression alone. (G–I) Wing discs expressing *UAS-HA-Krz* and *UAS-HrsRNAi* alone, or together, through the dorsal-compartment-specific *ap*-Gal4 combined with GFP were stained for Smo and HA. The arrow identifies the inhibition of Smo accumulation upon Krz expression, although Hrs RNAi was simultaneously expressed. Arrowheads indicate the mild accumulation of Smo upon Hrs RNAi expression. GFP in I indicates the RNAi expression domain of wing disc. (J) A wing disc expressing *UAS-HA-Krz* and *UAS-Vps32RNAi* driven by *ap*-Gal4 was stained for Smo and HA. The arrow indicates the high accumulation of Smo upon Vps32 RNAi expression, with Krz expressed simultaneously. (K) A wing disc carrying *hrs* mutant clones and expressing HA-Krz by *MS1096*-Gal4 was stained for Smo, GFP, and Ci. Arrow indicates Smo accumulation in *hrs* mutant cells, which was not inhibited by Krz. Arrowhead indicates the inhibition of Smo accumulation by Krz in *hrs* wild-type cells.

proteasome. We explored the possibility of an interaction of Krz with different forms of Smo that are representative of different compartments. We found that endogenous Krz strongly interacted with transfected Myc–Smo^{WT}, indicating that Krz and Smo were physically associated (Fig. 7A, lane 1, top panel). We further found that Krz interacted with Smo^{K42R} at a level comparable to Smo^{WT}, indicating that mutating the 42 lysine residues in the Smo C-tail did not change the overall association of Krz with Smo (Fig. 7A, lane 2, top panel). However, Krz interacted with Smo^{KKDE} and Smo^{FD} at significantly higher levels than with Smo^{WT}, suggesting that endoplasmic reticulum-localized Smo (mediated by the KKDE signal) and endocytosed Smo (promoted by the FDNPVY internalization signal) are favorably subjected to Krz-mediated trafficking (Fig. 7A, lanes 3,4, top panel, and quantification analysis in the right panel). These data suggest that Krz physically interacts with the endocytosed and endoplasmic reticulum-localized Smo to promote Smo degradation through lysosomes.

We found that the endogenous Krz protein was very stable and that its stability was not altered by Vps32 RNAi, MG132 (a potent proteasome inhibitor), BFA1 or Hh treatment, suggesting that the endogenous Krz does not undergo degradation through either the proteasome- or lysosome-mediated pathways (Fig. 7B). We also found that the endogenous Krz protein was stable and was expressed in the wing imaginal disc, with a slightly higher level in the wing pouch, but that no difference was observed between the A-compartment and P-compartment cells (Fig. 7C), suggesting that the expression or stability of Krz is not regulated by Hh. These data indicate that endogenous Krz is likely recycled before targeting Smo into the proteasome or lysosome, similar to what occurs for ubiquitin recycling in the endocytic pathway. The overexpressed Krz was also very stable and completely blocked Smo accumulation in P-compartment and A-compartment cells near the A/P boundary (Fig. 6G); however, Krz overexpression did not alter the expression levels of Ci, Ptc and En (Fig. 7D,E). These data indicate that the Smo internalized by Krz was active. This was further supported by the finding that overexpression of Krz did not block the accumulation of Cos2 and Fu, but rather increased the levels of Cos2 and Fu in P-compartment cells (Fig. S7A,B), which indicates that Krz neither inhibites Smo activity nor blocks Smo protein accumulation.

Journal of Cell Science (2018) 131, jcs211367. doi:10.1242/jcs.211367

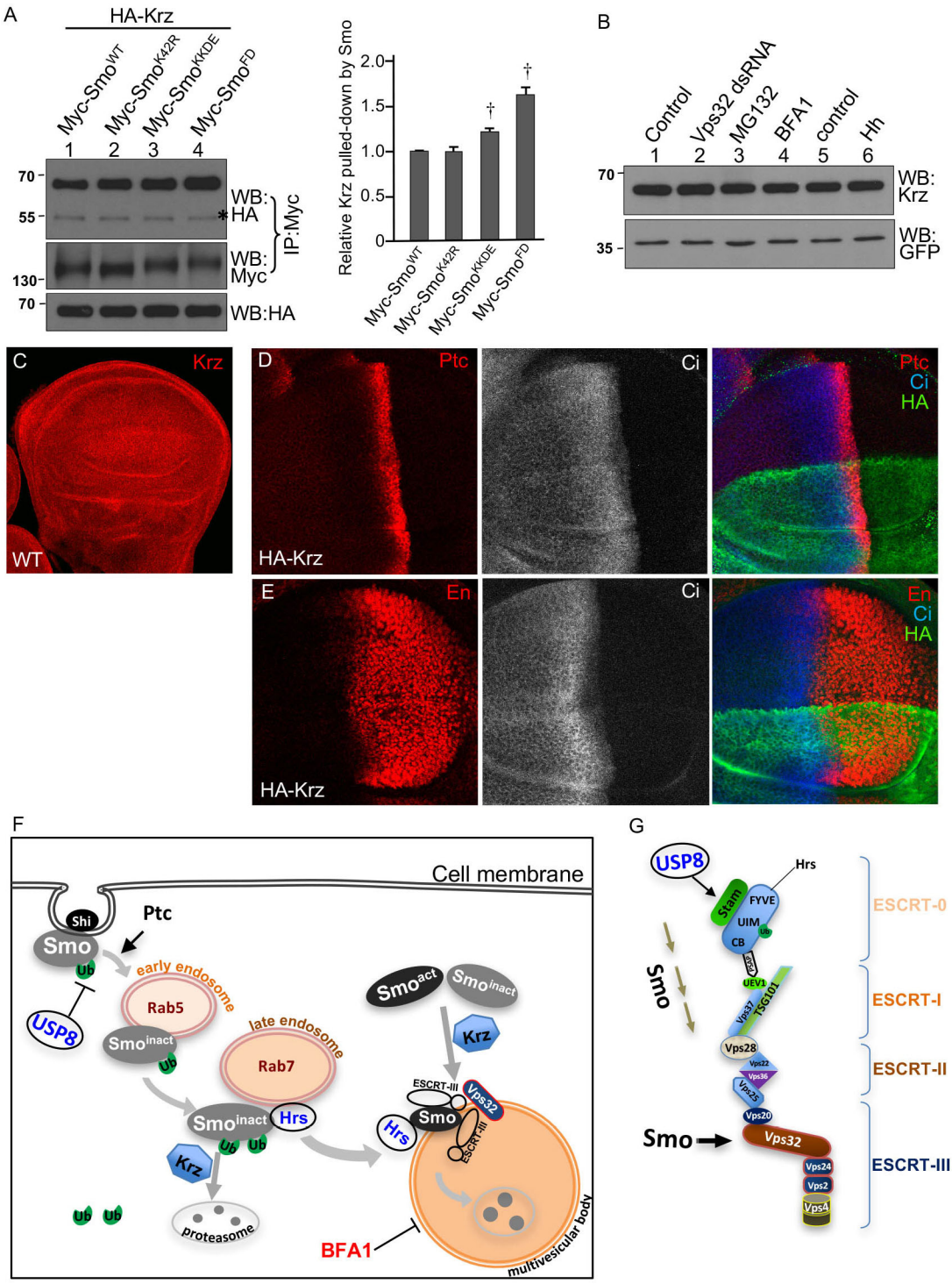

Fig. 7. See next page for legend.

DISCUSSION

The regulation of Smo activation has been widely studied, and mainly focused on the identification and characterization of Smo mutations, including those mutations shown in earlier studies to drive cancer formation (Taipale et al., 2000; Xie et al., 1998). It is unclear whether the accumulation of wild-type Smo under certain conditions can induce the activation of Hh signaling, and thus over-proliferation of cells. In addition, it is unclear whether and how Smo transduces Hh signaling inside the cell, although it has been demonstrated that accumulation of Smo at the cell surface (in *Drosophila*) or in cilia (in vertebrates) triggers the activation of Smo. In this study, we found that inactivation of the ESCRT-III complex caused severe accumulation of Smo in the MVB and dramatic activation of Hh signaling. In contrast, inactivation of other intracellular components, such as the ESCRTs 0–II, only induced a mild accumulation of Smo. By carrying out genetic epistasis analysis, and by examining the accumulation of different forms of Smo in different cellular compartments, we found that Krz acted in

Fig. 7. The physical interaction of Krz and different forms of Smo is enhanced by blocking Smo trafficking from the MVB to the lysosome. (A) A cell-based assay to examine different forms of Smo interaction with Krz. S2 cells were transfected with Myc–Smo^{WT}, Myc–Smo^{K42R}, Myc–Smo^{KKDE} or Myc–Smo^{FD}, together with HA–Krz, followed by immunoprecipitation (IP) with the anti-Myc antibody and analysis by western blotting (WB) using either the anti-HA antibody to determine the level of Smo-bound Krz or the anti-Myc antibody to monitor the expression of Smo. Smo was normalized by the methods described (see Materials and Methods). The asterisk indicates mouse IgG, which served as a loading control. Cell lysates were subjected to western blot analysis with the anti-HA antibody to monitor Krz expression, which also served as a loading and transfection control. Quantification of the amount of Krz associated with Smo variants is shown in the right panel. The signal density of Krz associated with Smo^{WT} was defined as 1. $^{\dagger}P<0.001$ versus interaction with Smo^{WT} in the first column (Student's *t*-test). Data were from three independent experiments. (B) S2 cells were treated with Vps32 dsRNA, MG132, BFA1 or HhN-conditioned medium. Cell lysates were subjected to western blot analysis using the anti-Krz antibody to examine the stability of the endogenous Krz protein. GFP served as a loading control. (C) A wild-type wing disc was stained with the anti-Krz antibody to examine the expression of Krz in the wing disc. (D,E) The excessively expressed Krz downregulates the accumulation of Smo but does not alter the activity of Hh signaling. Wing discs expressing *UAS-HA-Krz* driven by the *ap*-Gal4 were stained for HA, Ptc, Ci and En. HA–Krz was specifically expressed in the dorsal compartment cells but there were no differences in Ptc, Ci and En between dorsal and ventral compartment cells. (F) A model for Smo intracellular trafficking mechanisms uncovered in this study. Smo undergoes endocytosis through the early and late endosomes, which is mediated by ubiquitylation. USP8 prevents Smo ubiquitylation and elevates Smo cell surface accumulation. Smo^{inact} indicates the inactive forms of Smo. A parallel pathway is identified in this study, which is mediated by Krz to sort the inactive and active forms of Smo to the MVB and lysosome for degradation. Smo^{act} indicates the active forms of Smo. (G) A model for Smo sorting through the ESCRT complex. One way for Smo to accumulate in the ESCRT-III-containing/MVB compartments is the endocytosis pathway that involves ESCRT-0, ESCRT-I and ESCRT-II. The other pathway for Smo to accumulate in the ESCRT-III/MVB is mediated by Krz. Taken together, the inactivation of ESCRT-III consistently leads to the accumulation of high level of Smo, which can be activated by phosphorylation.

parallel with the ESCRTs 0–II pathway to promote Smo degradation through the MVB and lysosome. The Smo that accumulated upon the inactivation of ESCRT-III was highly active, which was likely induced by phosphorylation but not sumoylation. We propose a model for Smo intracellular trafficking regulated by different pathways (Fig. 7F,G). The findings in this study uncovered a novel mechanism for Smo activation in the intracellular compartment, raising the possibility for tissue over-proliferation caused by an excessive level of Smo induced by the malfunction of ESCRT-III.

The signaling of many GPCRs is controlled by endocytosis. There are incidents of endocytic regulation at the plasma membrane, regulation of signaling by different endocytic routes and signaling from endosomes (Sigismund et al., 2012). Models have been proposed for GPCR signaling in the endosomes. These include the sustained GPCR signaling from endosomes as is likely to occur for the thyroid-stimulating hormone GPCR (TSHR), and the acute GPCR signaling from endosomes for the D1 dopamine receptor (DRD1) (Irannejad and von Zastrow, 2014). It is not surprising that malfunction of the endosomal trafficking compartments causes Smo accumulation. It is also not surprising that Krz promotes Smo internalization. What is surprising is that Smo can accumulate in the MVB at such an unexpected level as to induce its phosphorylation and activation. It is also surprising that, independently of Ptc inhibition, the activated Smo induces high levels of Hh target gene expression. These findings suggest a model for GPCR activation in ESCRT-III-containing or MVB compartments.

In this study, we show that Krz mediates the internalization of Smo through a pathway parallel to the endosome/ESCRT-0-mediated endocytosis. However, there is no effect of *krz* loss-of-function on Smo accumulation and Hh signaling activity (Fig. 6E) (Li et al., 2012; Molnar et al., 2011). This has been puzzling for years. We provide the following explanations. It is possible that other arrestins compensate for the function of *krz* when *krz* is lost. It is also possible that Krz functions in parallel to the endocytosis pathway, allowing Smo to be degraded through other pathways when *krz* is lost. This latter idea is supported by findings in this study, and also supported by the finding that Krz acts in an ubiquitylation-independent manner to guide Smo to both proteasome- and lysosome-mediated degradation (Li et al., 2012). The third possibility is that endogenous Krz can only regulate the basal level of Smo trafficking and thus the basal degradation of Smo. Moreover, it is possible that Krz-mediated internalization of Smo does not alter the activity of Smo in the intracellular compartment. This hypothesis may explain, at least in part, why overexpressed Krz completely blocks Smo accumulation without any effect on Hh pathway activity (Fig. 7D,E).

MVB sorting is normally mediated by the ESCRT pathway, in which the MVB cargo selection is determined by the ESCRT 0–III protein complexes (Henne et al., 2011; Hurley and Hanson, 2010). ESCRTs 0–II contain ubiquitin-binding proteins and are responsible for the sequestration of ubiquitylated proteins. Hrs, containing a ubiquitin-interacting motif (UIM), forms a heterodimer with Stam to constitute ESCRT-0 complex. ESCRT-I contains Vps23, also known as tumor susceptibility gene 101 (Tsg101), which possesses a ubiquitin E2 variant (UEV) domain responsible for cargo recognition. ESCRT-II contains Vps36, which carries a GRAM-like ubiquitin-binding motif in EAP45 (GLUE) domain also responsible for cargo recognition. ESCRT-III, which does not bind ubiquitin directly, contains Vps32 and Vps20, assembles on endosomes and further connects with Vps4 for subsequent entrapment of GPCRs within the MVB. The ESCRT-III complex is pivotal to cargo capture into MVB (Wollert and Hurley, 2010). The ESCRT/MVB pathway is involved in the trafficking many proteins, and a recent study has found that ESCRT-III and Krz are involved in ligand-independent Notch signaling (Hori et al., 2011). From the view of Smo trafficking, ubiquitylated Smo can be recognized by ESCRT-0, -I, and -II, and can be clustered into the ESCRT-III-containing compartment after deubiquitylation. ESCRT-III does not bind ubiquitin, raising the possibility that Krz-mediated non-ubiquitylated forms of Smo can be sorted to the ESCRT-III-containing compartment with subsequent lysosomal degradation. We speculate that Smo is activated in the MVB independently of ubiquitylation and sumoylation regulation. In support this concept, we found that the accumulation of Smo upon inactivation of the ESCRT-III did not alter the ubiquitylation and sumoylation of Smo (Fig. 3F,G). The other supportive finding was that the active forms of Smo underwent lysosome-mediated degradation (Fig. 4D). Many lysine residues in the Smo C-tail can be either sumoylated or ubiquitylated (Li et al., 2012; Ma et al., 2016; Xia et al., 2012; Yang et al., 2013; Zhang et al., 2017). It is likely that Smo sumoylation counteracts ubiquitylation to regulate Smo cell surface activation; however, the intracellular activation of Smo does not require sumoylation or deubiquitylation. The intracellularly accumulated Smo was phosphorylated (Fig. 3D,E), which likely induces dimerization and activation of the protein.

It is interesting that the overexpressed Krz blocked Smo accumulation, but increased Fu and Cos2 accumulation in P-compartment cells (Fig. S7A,B). This indicates that the components

downstream of Smo are accumulated and likely activated by the overexpression of Krz, and suggests that Krz does not inhibit the activity of Smo, Cos2 and Fu, although Krz blocks Smo accumulation in wing disc. Upon examining the levels of Fu and Cos2 in the intracellular compartment, we found that Fu and Cos2 were not accumulated in cells with mutated *vps20* (Fig. S7C,D), suggesting that the accumulation and activation of Smo does not promote the accumulation of Fu and Cos2 in these cells. These data also suggest that Krz likely acts upstream of ESCRT-III to regulate Smo trafficking. Taken together with the finding that the intracellular activation of Smo does not require sumoylation, we speculate that the activation of Smo in the intracellular compartment is mediated in a different way from its activation on the cell surface.

MATERIALS AND METHODS

Constructs, mutants and transgenes

Generation of the Myc–Smo^{WT}, Myc–Smo^{SD123}, Myc–Smo^{PKA123} and Smo–CFP constructs was previously described (Jia et al., 2004; Liu et al., 2007). Myc–Smo^{KKDE} and Myc–Smo^{FD} were constructed by fusing one copy of the sorting signal KKDE or the 32-amino-acid peptide containing the FDNPVY signal to the Smo C-terminus, respectively. Myc-Smo^{K6R}, Myc-Smo^{K42R} and Myc-Smo^{KallR} were as described previously (Yang et al., 2013). HA–Ub, HA–SUMO and Flag–Ubc9 were as previously described (Xia et al., 2012; Zhang et al., 2017). To construct *tub*-Smo^{K42R}, *tub*-Smo^{KKDE} and *tub*-Smo^{FD}, the *tubulin-α* promoter was inserted upstream of the Smo^{K42R}, Smo^{KKDE} and Smo^{FD} sequence and subcloned into the attB-UAST vector (Xia et al., 2012). The HA–Krz construct and transgenic line have been described previously (Zhang et al., 2017). The HA–Ptc construct and transgenic line have been described previously (Jiang et al., 2016). All the transgenic lines were generated by using the 75B1 VK5-attP locus to ensure Smo protein expression at the same levels without positional effects.

The wing-specific *MS1096*-Gal4 and wing dorsal-compartment-specific *ap*-Gal4 have been described in our previous studies (Jia et al., 2010, 2003). *vps32^{G5}* and *vps32^{O3}* were obtained from Bloomington Stock Center (BSC) (#39635 and #39623, respectively), and *vps32* mutant clones shown in this study were generated by using the *vps32^{G5}* mutant combined with FRT42D. To generate survival clones, *UAS-P35* was expressed in wing disc through *MS1096*-Gal4. The HA–Krz transgenic insertion on the second chromosome and the *krz* mutant line have been described previously (Mukherjee et al., 2005). *krz* mutant clones were generated by using the *krz* mutant combined with FRT82B. *vps28* mutant clones were generated with the *vps28^{B9}-FRT42D* stock from BSC (#39634). Genotypes for examining the activity of the Smo transgene in *smo* clones were: *yw hsp-flp/+* or *Y*; *smo3 FRT40/hs-GFP FRT40*; *tub-Smo-variant/+*. Gal80^{ts} flies were from BSC (#7017 and #7108). Vps32 RNAi lines #38305 from BSC and v106823 from the Vienna *Drosophila* Research Center (VDRC) gave rise to similar phenotypes, thus v106823 was used for most of the experiments. The Hrs RNAi lines from Bloomington (#28026 and #28964) or VDRC (v20933) gave rise to similar phenotypes and were characterized in our previous study (Fan et al., 2013). The Vps32–GFP line from Dr Fen-Biao Gao (University of Massachusetts) and the Vps32–GFP line from BSC (#32559) consistently showed a dominant-negative effect in wing discs. The transgenic line with Vps4^{DN} carrying E232Q mutation was a gift from Drs Harald Stenmark and Tor Erik Rusten (Oslo University Hospital) (Rusten et al., 2007). The LAMP1–GFP line was a gift from Dr Helmut Kramer (UT Southwestern). The Krz RNAi line v41559 was from the VDRC and RNAi efficiency in wing disc was confirmed by use of anti-Krz antibody (1:50, PA1-730, Thermo Scientific) upon immunostaining of the wing disc. The Hh RNAi line v1402 was obtained from the VDRC and characterized in our previous studies. Beclin1 (also known as Atg6 and Vps30) RNAi (#28060), Vps34RNAi (#33384 and #64011), Vps15 RNAi (#34092 and #57011), Atg7 RNAi (#27707), Atg8a RNAi (#34340 and #28989) and Atg8b RNAi (#27554) were obtained from the BSC.

Immunostaining of the wing imaginal disc

Wing discs from third-instar larvae with specific genotypes were dissected in PBS then fixed with 4% formaldehyde in PBS for 20 min. After permeabilization with PBS supplemented with 1% Triton X-100 (PBST), discs were incubated with the indicated primary antibodies for 3 h and the appropriate secondary antibodies for 1 h, and washed three times with PBST after each incubation. For wing disc treatment, 300 nM BFA1 (Sigma) in M3 medium (Sigma; enriched with fly extract) was used and the discs were treated for 4 h before primary and secondary antibody staining. The same amount of DMSO in M3 medium was used as control. Primary antibodies used were: mouse anti-Myc (1:50; 9E10, Santa Cruz Biotechnology), anti-Flag (1:150; M2, Sigma), anti-HA (1:100; F7, Santa Cruz Biotechnology), anti-SmoN (1:10; DSHB), anti-En (1:10; DSHB), anti-Ptc (1:20, DSHB), anti-Ub-FK2 (1:50; PW1180, Enzo), anti-Cos2 (1:50; 5D6, gift from Dr David Robbins, University of Miami); rabbit anti-β-Gal (1:1500; Cappel), anti-SmoP (1:10; Fan et al., 2012), anti-Krz (1:50; PA1-730, Thermo Scientific), anti-GFP (1:200; #632377, Clonetech), anti-Rab7 (1:3000; gift from Dr Akira Nakamura, Department of Germline Development, Kumanoto University, Japan), anti-Fu (gift from Dr David Robbins), anti-Vps4 (gift from Dr Erik Rusten); rat anti-Ci (1:10; 2A1, DSHB), and guinea pig anti-Hrs (gift from Dr Hugo Bellen, Baylor College of Medicine, USA). Affinity-purified secondary antibodies (Jackson ImmunoResearch) for multiple labeling were used. Fluorescence signals were acquired on an Olympus confocal microscope and images processed with Olympus FV10-ASW v.3.1b software. About 15 imaginal discs were scored and three to five disc images were taken for each genotype. Nearly all wing discs exhibit the immunostaining phenotypes, and over 90% adult wings exhibit the indicated phenotypes.

Cell culture, immunoprecipitation, western blotting, luciferase reporter assay, cell surface staining, and statistical analysis

Drosophila S2 cells were cultured as previously described (Jiang et al., 2016). Briefly, S2 cells were transfected with various UAST constructs using the Effectene transfection reagent (Qiagen). At 48 h post transfection, cells were treated with lysis buffer (100 mM NaCl, 50 mM Tris-HCl pH 8.0, 1.5 mM EDTA, 10% glycerol, 1% NP-40, and protease inhibitor tablet; Roche), followed by centrifugation at 17,949 ***g*** for 10 min. For each sample, 6×10^6 cells were harvested and lysed in 450 µl lysate buffer. 50 µl was saved for direct western blots, with 4 µl for each load. The remaining 400 µl was used for an immunoprecipitation assay, generating 30 µl samples. For immunoprecipitation, the cell lysate was incubated with the correct primary antibody for 2 h, and beads of protein A ultralink resin were added (Thermo Scientific). Immunoprecipitated protein samples were resolved by SDS-PAGE and transferred onto PVDF membranes (Millipore) for western blotting, which was performed using the indicated antibodies and the enhanced chemiluminescence (ECL) protocol. To normalize the level of Smo, 50 µM MG132 and 15 mM NH_4Cl was used to block Smo degradation, and samples were normalized for loading (Fan et al., 2012). The use of HhN-conditioned medium has been previously described (Fan et al., 2012). For the ubiquitylation assay, S2 cells were transfected with Myc–Smo plus HA–Ub and lysed with denaturing buffer (1% SDS, 50 mM Tris-HCl pH 7.5, 0.5 mM EDTA, and 1 mM DTT) and incubated at 100°C for 5 min. The lysates were then diluted with regular lysis buffer and subjected to immunoprecipitation with the anti-Myc antibody and western blotting with the anti-HA antibody. Experimental protocols for MG132 (Calbiochem), a proteasome inhibitor, and NH_4Cl (Sigma-Aldrich), a lysosome inhibitor, to block Smo degradation have been previously described (Li et al., 2012; Xia et al., 2012). For BFA1 treatment, 300 nM BFA1 was added to the medium for 4 h before harvesting the cells. The S2 cell treatment with dsRNA has been described previously (Liu et al., 2007). dsRNA was synthesized against a specific region to knock down the following gene expression: Vps32-1 (nucleotides 7–566); Vps32-2 (nucleotides 559 to +460 after the stop codon in the 3′-UTR); Vps20 (nucleotides 21–530); Vps15 (nucleotides 1941–2531); Vps30 (nucleotides 691–1254); Vps34 (nucleotides 2279–2820), and RNAi efficiency for each RNAi was monitored by qRT-PCR. GFP dsRNA was synthesized against nucleotides 6–606 and was used as the control for most RNAi experiments. GFP RNAi efficiency was determined by western blotting using the anti-GFP antibody to detect the expression levels of co-transfected GFP. For qRT-PCR, total RNA was extracted with Trizol reagent (Invitrogen). cDNA was synthesized using SuperScript III First Strand Synthesis kit (Invitrogen)

according to the manufacturer's instructions. The quantitative real-time PCR reactions were carried out using SYBR Green PCR master mix reagents (Thermo Scientific) on the ABI StepOnePlus real-time PCR system (Applied Biosystems). Thermal cycling was conducted at 95°C for 30 s, followed by 40 cycles of amplification at 95°C for 5 s, 55°C for 30 s and 72°C for 15 s. The following primers were used: Vps32, 5′-GACGAACTGAATATAGCCCG-3′ and 5′-TCATGTCGTGCACCTTGTCC-3′; Vps20, 5′-GATGTGCCCA-CCGAAGATCT-3′ and 5′-CAGGACTTTCTTGGTTGCTT-3′.

The cell-based assay to examine Smo cell surface accumulation was carried out by immunostaining with the anti-SmoN antibody before cell permeabilization. After incubation with the anti-SmoN antibody at room temperature for 30 min, cells were washed with PBS and fixed with 4% formaldehyde in PBS for 20 min. After permeabilization with 1% PBST, cells were then incubated with the anti-Myc antibody for 1 h (unless autofluorescence of CFP was to be measured), appropriate secondary antibody for 1 h, washed three times with PBST after each incubation, and finally mounted on slides with 80% glycerol. For maximal Hh signal strength, a UAST–Hh construct was also included in the transfection (Fan et al., 2012). Fluorescence signals were acquired with the 60× objective on an Olympus confocal microscope. Smo density was analyzed with ImageJ software (NIH, version 1.48v).

For the *ptc-luc* reporter assay, S2 cells were cultured in six-well plates and transfected with 50 ng *tub-Ci*, 20 ng *renilla* and 150 ng *ptc-luc* reporter vectors. At 48 h post-transfection, cells were lysed for luciferase activity analysis with the dual-luciferase reporter assay system (Promega, Madison, WI). *Renilla* luciferase was used to normalize the luciferase activity. The measurements of dual-luciferase were determined with a GLOMAX Multi Detection System (Promega).

Presented data are representative of three experiments, with standard deviation (s.d.) bars generated from four replicates. For statistical analysis, Student's *t*-test was used for cell culture studies involving two independent groups.

Antibodies used in this study for western blotting were: mouse anti-Myc (1:5000; 9E10, Santa Cruz Biotechnology), anti-HA (1:1000; F7, Santa Cruz Biotechnology, anti-GFP (1:500; MAB3580, Millipore), rabbit anti-Myc (1:2000; A-14, Santa Cruz Biotechnology), anti-SmoP (1:50; Fan et al., 2012), and anti-Krz (1:2500; PA1-730, Thermo Scientific).

Acknowledgements
We thank the previous laboratory members including Hongge Jia, Junkai Fan, and Jingyi Liu for the initiation of this project and help with some of the experiments. We thank Dr Yun Zhao for the Smo^{K6R}, Smo^{K42R}, and Smo^{KallR} constructs, Dr David J. Robbins for the anti-Cos2 and anti-Fu antibodies, Dr Akira Nakamura for the anti-Rab7 antibody, and Dr Hugo Bellen for the anti-Hrs antibody. We thank Dr Markus Affolter for the $hrs^{-/-}$ and $hrs^{-/-}$; $stam^{-/-}$ mutants, Dr Thomas Vaccari for the $vps20^{-/-}$ mutant, Dr Spyros Artavanis-Tsakonas for the $krz^{-/-}$ mutant and *UAS-Krz* transgenic line, Dr Fen-Biao Gao for the Vps32–GFP line, Drs Harald Stenmark and Tor Erik Rusten for the $Vps4^{DN}$ line and the anti-Vps4 antibody, and Dr Helmut Kramer for the LAMP1–GFP line. We also thank the BSC, VDRC, and TRiP at Harvard Medical School for fly stocks, the Developmental Studies Hybridoma Bank for antibodies. We are grateful to Heather N. Russel-Simmons for critically reading the manuscript.

Competing interests
The authors declare no competing or financial interests.

Author contributions
Conceptualization: J.J.; Methodology: K.J., Y.L., J.Z., J.J.; Formal analysis: K.J., Y.L., J.Z., J.J.; Investigation: J.J.; Resources: J.J.; Data curation: K.J., Y.L., J.Z.; Writing - original draft: K.J., J.J.; Writing - review & editing: J.J.; Supervision: J.J.; Funding acquisition: J.J.

Funding
This study was supported by National Institutes of Health (grant R01 GM079684 and pilot grant P30 CA177558) to J.J. We also thank the Shared Resource Facilities of the University of Kentucky Markey Cancer Center (P30 CA177558), and acknowledge the Imaging Core of the COBRE (P20 GM121327). Deposited in PMC for release after 12 months.

Supplementary information
Supplementary information available online at
http://jcs.biologists.org/lookup/doi/10.1242/jcs.211367.supplemental

References
Briscoe, J. and Thérond, P. P. (2013). The mechanisms of Hedgehog signalling and its roles in development and disease. *Nat. Rev. Mol. Cell Biol.* **14**, 418-431.
Chen, Y. and Jiang, J. (2013). Decoding the phosphorylation code in Hedgehog signal transduction. *Cell Res.* **23**, 186-200.
Fan, J., Liu, Y. and Jia, J. (2012). Hh-induced Smoothened conformational switch is mediated by differential phosphorylation at its C-terminal tail in a dose- and position-dependent manner. *Dev. Biol.* **366**, 172-184.
Fan, J., Jiang, K., Liu, Y. and Jia, J. (2013). Hrs promotes ubiquitination and mediates endosomal trafficking of smoothened in Drosophila hedgehog signaling. *PLoS ONE* **8**, e79021.
Funderburk, S. F., Wang, Q. J. and Yue, Z. (2010). The Beclin 1-VPS34 complex–at the crossroads of autophagy and beyond. *Trends Cell Biol.* **20**, 355-362.
Goh, L. K., Huang, F., Kim, W., Gygi, S. and Sorkin, A. (2010). Multiple mechanisms collectively regulate clathrin-mediated endocytosis of the epidermal growth factor receptor. *J. Cell Biol.* **189**, 871-883.
Henne, W. M., Buchkovich, N. J. and Emr, S. D. (2011). The ESCRT pathway. *Dev. Cell* **21**, 77-91.
Hooper, J. E. and Scott, M. P. (2005). Communicating with Hedgehogs. *Nat. Rev. Mol. Cell Biol.* **6**, 306-317.
Hori, K., Sen, A., Kirchhausen, T. and Artavanis-Tsakonas, S. (2011). Synergy between the ESCRT-III complex and Deltex defines a ligand-independent Notch signal. *J. Cell Biol.* **195**, 1005-1015.
Hurley, J. H. and Hanson, P. I. (2010). Membrane budding and scission by the ESCRT machinery: it's all in the neck. *Nat. Rev. Mol. Cell Biol.* **11**, 556-566.
Irannejad, R. and von Zastrow, M. (2014). GPCR signaling along the endocytic pathway. *Curr. Opin. Cell Biol.* **27**, 109-116.
Jia, J. and Jiang, J. (2006). Decoding the Hedgehog signal in animal development. *Cell. Mol. Life Sci.* **63**, 1249-1265.
Jia, J., Tong, C. and Jiang, J. (2003). Smoothened transduces Hedgehog signal by physically interacting with Costal2/Fused complex through its C-terminal tail. *Genes Dev.* **17**, 2709-2720.
Jia, J., Tong, C., Wang, B., Luo, L. and Jiang, J. (2004). Hedgehog signalling activity of Smoothened requires phosphorylation by protein kinase A and casein kinase I. *Nature* **432**, 1045-1050.
Jia, H., Liu, Y., Xia, R., Tong, C., Yue, T., Jiang, J. and Jia, J. (2010). Casein kinase 2 promotes Hedgehog signaling by regulating both smoothened and Cubitus interruptus. *J. Biol. Chem.* **285**, 37218-37226.
Jiang, J. and Hui, C.-C. (2008). Hedgehog signaling in development and cancer. *Dev. Cell* **15**, 801-812.
Jiang, K. and Jia, J. (2015). Smoothened regulation in response to Hedgehog stimulation. *Front. Biol.* **10**, 475-486.
Jiang, K., Liu, Y., Fan, J., Epperly, G., Gao, T., Jiang, J. and Jia, J. (2014). Hedgehog-regulated atypical PKC promotes phosphorylation and activation of Smoothened and Cubitus interruptus in Drosophila. *Proc. Natl. Acad. Sci. USA* **111**, E4842-E4850.
Jiang, K., Liu, Y., Fan, J., Zhang, J., Li, X.-A., Evers, B. M., Zhu, H. and Jia, J. (2016). PI(4)P promotes phosphorylation and conformational change of smoothened through interaction with its C-terminal tail. *PLoS Biol.* **14**, e1002375.
Li, S., Chen, Y., Shi, Q., Yue, T., Wang, B. and Jiang, J. (2012). Hedgehog-regulated ubiquitination controls smoothened trafficking and cell surface expression in Drosophila. *PLoS Biol.* **10**, e1001239.
Liu, Y., Cao, X., Jiang, J. and Jia, J. (2007). Fused Costal2 protein complex regulates Hedgehog-induced Smo phosphorylation and cell-surface accumulation. *Genes Dev.* **21**, 1949-1963.
Ma, G., Li, S., Han, Y., Li, S., Yue, T., Wang, B. and Jiang, J. (2016). Regulation of smoothened trafficking and hedgehog signaling by the SUMO pathway. *Dev. Cell* **39**, 438-451.
Molnar, C., Ruiz-Gómez, A., Martín, M., Rojo-Berciano, S., Mayor, F. and de Celis, J. F. (2011). Role of the Drosophila non-visual ß-arrestin kurtz in hedgehog signalling. *PLoS Genet.* **7**, e1001335.
Mukherjee, A., Veraksa, A., Bauer, A., Rosse, C., Camonis, J. and Artavanis-Tsakonas, S. (2005). Regulation of Notch signalling by non-visual beta-arrestin. *Nat. Cell Biol.* **7**, 1191-1201.
Pak, E. and Segal, R. A. (2016). Hedgehog signal transduction: key players, oncogenic drivers, and cancer therapy. *Dev. Cell* **38**, 333-344.
Pulipparacharuvil, S., Akbar, M. A., Ray, S., Sevrioukov, E. A., Haberman, A. S., Rohrer, J. and Kramer, H. (2005). Drosophila Vps16A is required for trafficking to lysosomes and biogenesis of pigment granules. *J. Cell Sci.* **118**, 3663-3673.
Raiborg, C. and Stenmark, H. (2009). The ESCRT machinery in endosomal sorting of ubiquitylated membrane proteins. *Nature* **458**, 445-452.
Rodahl, L. M., Haglund, K., Sem-Jacobsen, C., Wendler, F., Vincent, J.-P., Lindmo, K., Rusten, T. E. and Stenmark, H. (2009). Disruption of Vps4 and JNK function in Drosophila causes tumour growth. *PLoS ONE* **4**, e4354.
Rusten, T. E., Vaccari, T., Lindmo, K., Rodahl, L. M. W., Nezis, I. P., Sem-Jacobsen, C., Wendler, F., Vincent, J.-P., Brech, A., Bilder, D. et al. (2007). ESCRTs and Fab1 regulate distinct steps of autophagy. *Curr. Biol.* **17**, 1817-1825.

Sigismund, S., Confalonieri, S., Ciliberto, A., Polo, S., Scita, G. and Di Fiore, P. P. (2012). Endocytosis and signaling: cell logistics shape the eukaryotic cell plan. *Physiol. Rev.* **92**, 273-366.
Sorkin, A. and von Zastrow, M. (2009). Endocytosis and signalling: intertwining molecular networks. *Nat. Rev. Mol. Cell Biol.* **10**, 609-622.
Sweeney, N. T., Brenman, J. E., Jan, Y. N. and Gao, F.-B. (2006). The coiled-coil protein shrub controls neuronal morphogenesis in Drosophila. *Curr. Biol.* **16**, 1006-1011.
Taipale, J., Chen, J. K., Cooper, M. K., Wang, B., Mann, R. K., Milenkovic, L., Scott, M. P. and Beachy, P. A. (2000). Effects of oncogenic mutations in Smoothened and Patched can be reversed by cyclopamine. *Nature* **406**, 1005-1009.
Wang, W. and Struhl, G. (2004). Drosophila Epsin mediates a select endocytic pathway that DSL ligands must enter to activate Notch. *Development* **131**, 5367-5380.
Williams, R. L. and Urbé, S. (2007). The emerging shape of the ESCRT machinery. *Nat. Rev. Mol. Cell Biol.* **8**, 355-368.
Wollert, T. and Hurley, J. H. (2010). Molecular mechanism of multivesicular body biogenesis by ESCRT complexes. *Nature* **464**, 864-869.
Xia, R., Jia, H., Fan, J., Liu, Y. and Jia, J. (2012). USP8 promotes smoothened signaling by preventing its ubiquitination and changing its subcellular localization. *PLoS Biol.* **10**, e1001238.
Xie, J., Murone, M., Luoh, S.-M., Ryan, A., Gu, Q., Zhang, C., Bonifas, J. M., Lam, C.-W., Hynes, M., Goddard, A. et al. (1998). Activating Smoothened mutations in sporadic basal-cell carcinoma. *Nature* **391**, 90-92.
Yang, X., Mao, F., Lv, X., Zhang, Z., Fu, L., Lu, Y., Wu, W., Zhou, Z., Zhang, L. and Zhao, Y. (2013). Drosophila Vps36 regulates Smo trafficking in Hedgehog signaling. *J. Cell Sci.* **126**, 4230-4238.
Zhang, J., Liu, Y., Jiang, K. and Jia, J. (2017). SUMO regulates the activity of Smoothened and Costal-2 in Drosophila Hedgehog signaling. *Sci. Rep.* **7**, 42749.
Zhao, Y., Tong, C. and Jiang, J. (2007). Transducing the Hedgehog signal across the plasma membrane. *Fly* **1**, 333-336.
Zhu, A. J., Zheng, L., Suyama, K. and Scott, M. P. (2003). Altered localization of Drosophila Smoothened protein activates Hedgehog signal transduction. *Genes Dev.* **17**, 1240-1252.